JPE 8-1-2

# New Control Scheme for the Wind-Driven Doubly Fed Induction Generator under Normal and Abnormal Grid Voltage Conditions

Osama S. Ebrahim †, Praveen K. Jain* and Goel Nishith**

†*Energy and Power Electronics Applied Research Lab (*e*PEARL), Queen's University, ON, Canada
**Cistel Technology, Ottawa, ON, Canada

## ABSTRACT

The wind-driven doubly fed induction generator (DFIG) is currently under pressure to be more grid-compatible. The main concern is the fault ride-through (FRT) requirement to keep the generator connected to the grid during faults. In response to this, the paper introduces a novel model and new control scheme for the DFIG. The model provides a means of direct stator power control and considers the stator transients. On the basis of the derived model, a robust linear quadratic (LQ) controller is synthesized. The control law has proportional and integral actions and takes account of one sample delay in the input owing to the microprocessor's execution time. Further, the influence of the grid voltage imperfection is mitigated using frequency shaped cost functional method. Compensation of the rotor current pulsations is proposed to improve the FRT capability as well as the generator performance under grid voltage unbalance. As a consequence, the control system can achieve i) fast direct power control without instability risk, ii) alleviation of the problems associated with the DFIG operation under unbalanced grid voltage, and iii) high probability of successful grid FRT. The effectiveness of the proposed solution is confirmed through simulation studies on 2MW DFIG.

**Keywords:** doubly fed induction generator, direct power control, linear quadratic regulator, frequency shaped cost function, fault ride-through, grid voltage unbalance, wind energy

## 1. Introduction

Global environmental concerns and the ever increasing need for energy, coupled with the steady progress in renewable energy technologies, are opening favorable opportunities for utilization of renewable energy resources. In particular, wind energy has experienced remarkable growth in the last few years, due in part to renewed public support and maturing turbine technologies [1]. A common configuration for large wind turbines is based on doubly fed induction generator (DFIG) with back to back converters between the AC grid and the rotor winding as shown in Fig. 1. The main advantage of the DFIG is the ability of variable speed operation with only 20-30% of the generated power having to pass through the power converters. This yields considerable reduction in the converter size which translates to substantial system cost benefit compared with the conversion of full power [2-4].

Modeling and control of the DFIG-based wind turbines

Manuscript received July 26, 2007; revised Oct. 12, 2007
† Corresponding Author: bayoumyo@post.queensu.ca
Tel: +1-613-533-2925; Fax: +1-613-533-6615, Queen's Univ.
* Queen's University, ON, Canada
** Cistel Technology, Ottawa, ON, Canada

under normal grid conditions have been extensively addressed in literature [3-8]. The stator active and reactive powers are conventionally regulated using rotor current vector control method with either stator voltage or stator flux orientation[9]. Furthermore, additional lead-lag compensators or dual rotor current control has been proposed to enhance the DFIG performance under grid voltage unbalance [10][11]. In both cases, the control system was dealing with slow dynamics or small transients and therefore; the necessity of fast rotor current control is not pronounced. However, penetration of wind power into electric grids has the potential for updating the existing grid codes to ensure secure power system operation [12]. In accordance to the new grid codes, the wind turbines have to withstand the most likely unbalanced faults as well as symmetrical 3-phase short circuits near the grid connection point [13]. A typical fault ride-through (FRT) requirements based on a time voltage diagram is shown in Fig. 2. The shaded area indicates the minimum voltage swing over which the wind turbine must remain online and tripping the generator or application of the crowbar protection is not permissible[14]. This new stricter regulation has presented a challenge for the DFIG based wind turbines because a sudden drop in the grid voltage causes a large current to flow in the rotor and limitation of this current is essential. One cost effective solution is to limit the rotor overcurrent during gird faults using the control system in the rotor-connected converter [15].

Accordingly, successful grid FRT could be obtained without increasing the converter rating. However, this basically requires fast response of the rotor current while maintaining the system stability. The traditional design of the rotor current control assumes ideal grid voltage and neglects the stator transients[5], [7], [10]. A stability investigation showed that the DFIG has two poorly damped poles near the supply frequency owing to stator transients and the system is unstable for certain operating conditions [16-18]. In reference [19], a feed-forward active compensation is suggested to make the system stability independent of the bandwidth of the rotor current control. Implementation of this technique requires information of the machine parameters and therefore, the system performance will deteriorate when the actual parameters differ from those values used in the control system. In particular, variation of the magnetizing inductance will be significant during voltage dips.

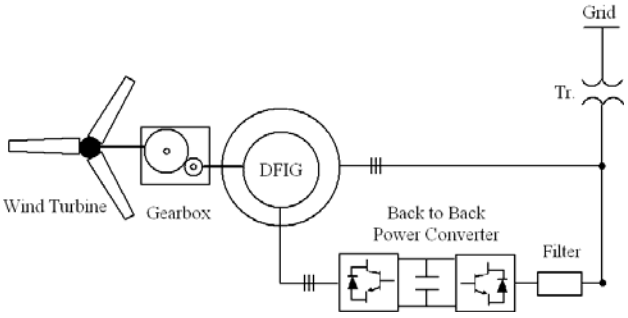


Fig. 1 DFIG-based variable speed wind turbine

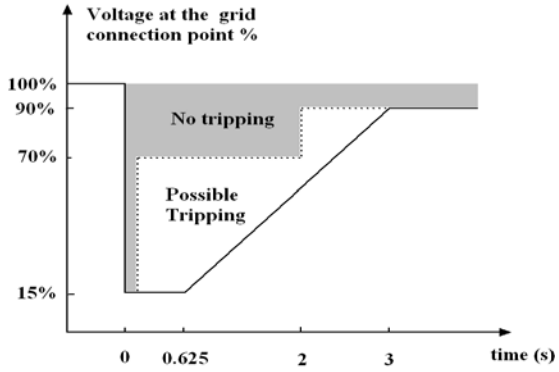


Fig. 2 Typical FRT standard [14]

In reference [15], an additional control loop is suggested to damp out the stator flux transient component and hence, limit the rotor current during fault conditions. Apart from the above mentioned limitations of the traditional rotor current control, pure integrator and differentiator are utilized to identify the transient component of the stator flux. It is known that such type of signal processing is associated with real-time implementation problems, especially if the level of the manipulated signal was small and polluted with harmonics [20]. Unfortunately, attempts to overcome these difficulties result in a phase shift error (i.e., delay). Even a small phase shift can deteriorate the system performance since it basically depends on the estimation accuracy and the speed of response.

Modern control algorithms can improve the DFIG performance by enhancing the dynamic response without a stability problem. Among these methods, the state space control is essentially suited for multi-input, multi-output

plants with limited stability margin and coupling between variables. The main contribution of this work is to introduce a new control methodology for the DFIG that can overcome the above mentioned difficulties. The method is described in the paper as follows. In section 2, a novel model for the DFIG is derived in the synchronous reference frame whose direct axis is aligned to the stator voltage vector. The model describes the DFIG as a two-input, two-output controlled object. The two output variables are the stator active and reactive power, while the two input variables are the rotor control voltage components. In section 3, a brief description of the DFIG performance under grid faults is introduced. Attenuation of the rotor current pulsations is proposed to improve the FRT capability and remove the difficulties of estimation of the stator flux transient component. In section 4, a robust LQ direct power controller is synthesized. The system output pulsations during abnormal grid voltage conditions are rejected using the frequency shaped cost functional method [21]. In section 5, a number of choices of disturbance rejection control objectives are realized and a suitable filter is designed. In order to validate the proposed control strategy, section 6 presents simulation results of 2MW DFIG-based wind turbine under balanced, unbalanced, and fault grid events. Conclusions are given in section 7.

## 2. Stator Power Model

The voltage equations of the DFIG can be expressed in the synchronous (d-q) reference frame as

$$\boldsymbol{V}_s = R_s \boldsymbol{I}_s + \frac{d\boldsymbol{\psi}_s}{dt} + j\omega_e \boldsymbol{\psi}_s \tag{1}$$

$$\boldsymbol{V}_r = R_r \boldsymbol{I}_r + \frac{d\boldsymbol{\psi}_r}{dt} + j\omega_s \boldsymbol{\psi}_r \tag{2}$$

$$\boldsymbol{\psi}_s = L_s \boldsymbol{I}_s + L_m \boldsymbol{I}_r \tag{3}$$

$$\boldsymbol{\psi}_r = L_m \boldsymbol{I}_s + L_r \boldsymbol{I}_r \tag{4}$$

Where,

$\boldsymbol{V}_s$, $\boldsymbol{V}_r$ are the stator, rotor voltage vectors.

$\boldsymbol{I}_s$, $\boldsymbol{I}_r$ are the stator, rotor voltage vectors.

$\boldsymbol{\psi}_s$, $\boldsymbol{\psi}_r$ are the stator, rotor flux linkage vectors.

$R_s$, $R_r$ are the stator, rotor resistances.

$L_s$, $L_r$ are the stator, rotor self inductances.

While $L_m$ is the magnetizing inductance and the symbols $\omega_e$, $\omega_r$, and $\omega_s = \omega_e - \omega_r$ denote the synchronous, rotor, and slip angular speed, respectively.

The expression of the stator apparent power is

$$S_s = P_s + jQ_s = \boldsymbol{V}_s \bullet \boldsymbol{I}_s^* \tag{5}$$

Here, $S_s$, $P_s$, and $Q_s$ are the stator apparent, active, and reactive power, respectively. The superscript "*" denotes the complex conjugate and the symbol "•" stands for the dot product.

As shown in Fig. 3, the stator voltage vector is selected to be aligned to the d-axis of the synchronous frame, i.e.

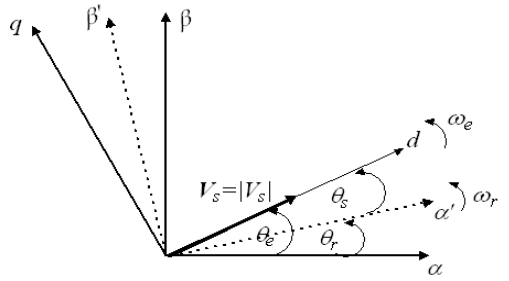


Fig. 3 Orientation of the stator voltage vector

$$\boldsymbol{V}_s = \left|\boldsymbol{V}_s\right| \tag{6}$$

Due to stator voltage orientation, (6) is valid under balanced, unbalanced, and transient stator voltage conditions.

The time derivative of the stator apparent power can be written as

$$\frac{dS_s}{dt} = \left|V_s\right| \frac{d\boldsymbol{I}_s^*}{dt} + \boldsymbol{I}_s^* \frac{d\left|V_s\right|}{dt} \tag{7}$$

At steady state, (7) will be vanished only under balanced stator voltage conditions.

The time derivative of the stator current can be deduced from (1)-(4) as

$$\frac{d\boldsymbol{I}_s}{dt} = (\frac{\gamma_r - j\omega_r}{\sigma L_s})\boldsymbol{\psi}_s - (\frac{\gamma_s + \gamma_r}{\sigma} + j\omega_s)\boldsymbol{I}_s - \frac{L_m}{\sigma L_s L_r}\boldsymbol{V}_r + \frac{|V_s|}{\sigma L_s} \quad (8)$$

The coefficients $\gamma_s$, $\gamma_r$ and $\sigma$ are defined by

$$\gamma_s = \frac{R_s}{L_s}, \quad \gamma_r = \frac{R_r}{L_r}, \quad \sigma = 1 - \frac{L_m^2}{L_s L_r} \quad (9)$$

Substitution from (8) into (7) gives

$$\frac{dS_s}{dt} = (-\frac{\gamma_s + \gamma_r}{\sigma} + j\omega_s)S_s + |V_s| \times (\frac{\gamma_r + j\omega_r}{\sigma L_s})\boldsymbol{\psi}_s^* - \frac{V_s L_m}{\sigma L_s L_r}\boldsymbol{V}_r^* + \frac{|V_s|^2}{\sigma L_s} + \boldsymbol{I}_s^* \frac{d|V_s|}{dt} \quad (10)$$

If the stator resistance is neglected, resolving (1) and (10) into their real and imaginary components yields

$$\frac{dP_s}{dt} = -\frac{\gamma_r}{\sigma}P_s - \omega_s Q_s + \frac{\gamma_r |V_s|}{\sigma L_s}\psi_{sd} + \frac{\omega_r |V_s|}{\sigma L_s}\psi_{sq} - \frac{L_m |V_s|}{\sigma L_s L_r}v_{rd} + \frac{|V_s|^2}{\sigma L_s} + i_{sd}\frac{d|V_s|}{dt} \quad (11)$$

$$\frac{dQ_s}{dt} = \omega_s P_s - \frac{\gamma_r}{\sigma}Q_s + \frac{\omega_r |V_s|}{\sigma L_s}\psi_{sd} - \frac{\gamma_r |V_s|}{\sigma L_s}\psi_{sq} + \frac{L_m |V_s|}{\sigma L_s L_r}v_{rq} - i_{sq}\frac{d|V_s|}{dt} \quad (12)$$

$$\frac{d\psi_{sd}}{dt} = \omega_e \psi_{sq} + |V_s| \quad (13)$$

$$\frac{d\psi_{sq}}{dt} = -\omega_e \psi_{sd} \quad (14)$$

Equations (11)-(14) are not suitable for the state control design. This difficulty can be cured by expressing the magnitude of the stator voltage as a sum of nominal value $V_{s0}$ and a small perturbed value $\widetilde{V}_s$

$$|V_s| = V_{s0} + \widetilde{V}_s \quad (15)$$

Further, due to high wind turbine inertia, one can assume that the mechanical transients are much slower than the electrical transients, i.e., $\omega_r \approx const \Rightarrow \omega_s \approx const$ . Accordingly, a linearized discrete-time state space model can be obtained from (11)-(15) as

$$x_p(k+1) = A_p\, x_p(k) + B_p u(k) + \xi(k)$$
$$y(k) = C_p x_p(k) \quad (16)$$

Here, $A_p$, $B_p$, and $C_p$ are constant matrices with proper dimensions while $\xi$ accounts for a process input disturbance due to grid voltage imperfection. The state $x_p$, input $u$, and output variable $y$ at the $k^{th}$ sampling instant are specified as in (17) where the superscript "T" denotes transposition.

$$x_p(k) = \begin{bmatrix} P_s(k) & Q_s(k) & \psi_{sd}(k) & \psi_{sq}(k) \end{bmatrix}^T$$
$$u(k) = \begin{bmatrix} v_{rd}(k) \\ v_{rq}(k) \end{bmatrix}, \; y(k) = \begin{bmatrix} P_s(k) \\ Q_s(k) \end{bmatrix} \quad (17)$$

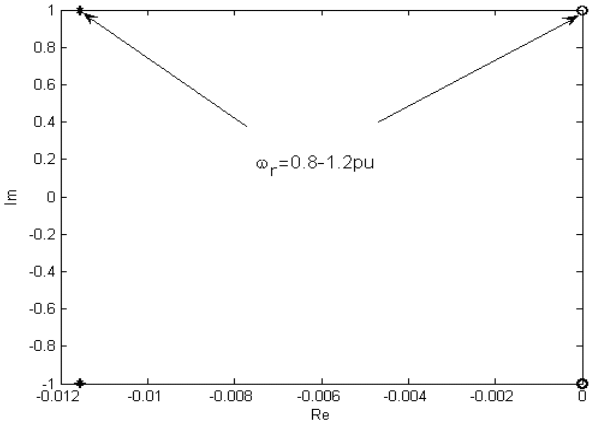


Fig. 4 s-plane loci of the poorly damped poles. (*) voltage model and (○) the power model

The main advantage of (16) is that it provides a means of direct stator power control without neglecting the stator transients. For the DFIG whose parameters are listed in the appendix , Fig. 4 shows the complex s-plane loci of the two poorly damped poles of the voltage model, (1)-(4), and of the power model, (11)-(14) after linearization, for a normal rotor operating speed range of 0.8- 1.2pu. In both cases, the poles locations are trivially dependent on the rotor speed.

## 3. DFIG under Grid Faults

The rotor voltage equation can be expressed in the rotor ($\alpha'\beta'$) reference frame as

$$\boldsymbol{V}_r = R_r \boldsymbol{I}_r + \frac{d\boldsymbol{\psi}_r}{dt} \tag{18}$$

The rotor flux linkage is related to the stator flux linkage by

$$\boldsymbol{\psi}_r = \frac{L_m}{L_s}\boldsymbol{\psi}_s + \sigma L_r \boldsymbol{I}_r \tag{19}$$

Substitution of (19) into (18) gives

$$\boldsymbol{V}_r = R_r \boldsymbol{I}_r + \sigma L_r \frac{d\boldsymbol{I}_r}{dt} + \frac{L_m}{L_s}\frac{d\boldsymbol{\psi}_s}{dt} \tag{20}$$

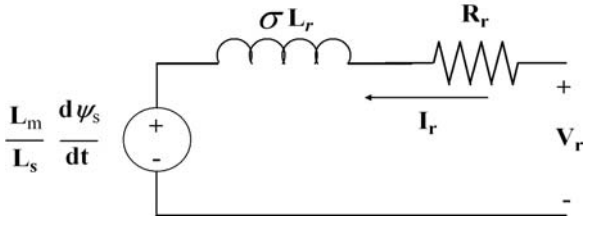


Fig. 5 DFIG equivalent circuit

Figure 5 shows the DFIG equivalent circuit as viewed from the rotor side based on (20). The rotor current is jointly determined by the rotor voltage and the derivative of the stator flux with time. Under symmetrical 3-phase fault on the grid side, the stator voltage will be depressed abruptly. As a consequence, the stator flux will have transient and steady state components causing transient and steady state current components to flow in the rotor winding. Due to small rotor resistance and leakage inductance, the rotor current will be effectively high. In reference [15], an additional rotor current control loop has been suggested to damp out the transient component of the stator flux; hence reducing the rotor fault current. Instead, direct attenuation of the rotor transient current is proposed in this work. This has the advantage of removing the difficulties associated with the online identification of the stator flux transient component which are listed in section 1.

In the synchronous frame, the transient component of the rotor current will be viewed as pulsations at the supply frequency $\omega_e$ in case of a sudden drop in the stator voltage due to a symmetrical 3-phase grid fault. Whereas, under asymmetrical grid faults (assuming no zero sequence), the stator voltage will have negative sequence component. As a result, the rotor current pulsations will be seen at frequency $2\omega_e$.

## 4. Proposed LQ Control

The system output oscillations at discrete frequency represent, in the control terminology, narrowband disturbance. The LQ/LQG control is effective for rejecting static disturbance or when the disturbance is well approximated by broadband Gaussian noise.

Consequently, the LQ control method must be modified to get good disturbance rejection without injecting excessive control energy into other frequency bands. An effective solution for treating this problem in the LQ control is the frequency shaped cost functional method [21]. In this method, the plant output is filtered using a filter ($A_f$, $B_f$, $C_f$) having poles at $\pm j\Omega$ where $\Omega$ is the frequency which the disturbance lies in.

The filter output $y_f$ is modeled in terms of the filter state $x_f$ as

$$\begin{aligned} x_f(k+1) &= A_f\, x_f(k) + B_f\, y(k) \\ y_f(k) &= C_f\, x_f(k) \end{aligned} \tag{21}$$

This is augmented with the plant model (16) to give

$$\begin{bmatrix} x_f(k+1) \\ x_p(k+1) \end{bmatrix} = \begin{bmatrix} A_f & B_f C_p \\ \mathbf{0} & A_p \end{bmatrix} \begin{bmatrix} x_f(k) \\ x_p(k) \end{bmatrix} + \begin{bmatrix} \mathbf{0} \\ B_p \end{bmatrix} u(k) + \begin{bmatrix} \mathbf{0} \\ I \end{bmatrix} \xi(k)$$

$$y(k) = \begin{bmatrix} 0 & C_p \end{bmatrix} \begin{bmatrix} x_f(k) \\ x_p(k) \end{bmatrix}$$

or

$$\begin{aligned} x(k+1) &= A\,x(k) + Bu(k-1) \\ y(k) &= C\,x(k) \end{aligned} \tag{22}$$

Equation (22) constitutes the state space model used for the control design where the matrix of the feedback gains can now be calculated by solving the standard LQ control problem. The control input vector is delayed by one sample period to compensate the microprocessor execution time. Furthermore, only feedback control will be considered in the following design steps and therefore $\xi(k)$ is omitted.

To get output track capability and zero steady state errors in the presence of parameter variations and modeling mismatch, the LQ control can be extended to include proportional and integral actions by defining an error signal as

$$\varepsilon(k) = R(k) - y(k) \tag{23}$$

Where, $R(k) = \begin{bmatrix} P_s^d(k) & Q_s^d(k) \end{bmatrix}^T$ is the desired output state vector.

An error system, describing the dynamics of the errors, can be constructed on the basis of (22) and (23) as [22-23]

$$X(k+1) = \Phi\, X(k) + \Gamma\, \Delta u(k) \tag{24}$$

Where,

$$\Phi = \begin{bmatrix} I & I & \mathbf{0} & \mathbf{0} \\ \mathbf{0} & I & C(I-A) & -CB \\ \mathbf{0} & \mathbf{0} & A & B \\ \mathbf{0} & \mathbf{0} & \mathbf{0} & \mathbf{0} \end{bmatrix}, \quad \Gamma = \begin{bmatrix} \mathbf{0} \\ \mathbf{0} \\ \mathbf{0} \\ I \end{bmatrix}, \tag{25}$$

$$X(k) = \begin{bmatrix} \varepsilon(k-1) & \Delta\varepsilon(k) & \Delta x(k) & \Delta u(k) \end{bmatrix}^T$$

The symbol $I$ denotes an identity matrix with proper dimension while $\Delta$ stands for the first difference operator. A quadratic performance index $J$ is selected as

$$J = \sum_{k=0}^{\infty} X(k+1)^T Q X(k+1) + \Delta u(k)^T \Re \Delta u(k) \tag{26}$$

The weighting matrices $Q$ and $\Re$ are symmetric positive semi definite and positive definite, respectively. The closed loop performance of the LQ regulator based design depends on the specifications of the weighting matrices. Considering,

$$\begin{aligned} \varepsilon(k) &= \varepsilon(k-1) + \Delta\varepsilon(k) \\ &= X(k)\big|_{(1,1)} + X(k)\big|_{(1,2)} \end{aligned} \tag{27}$$

the following structure can be suggested

$$Q(14x14) = \begin{bmatrix} qI & qI & \mathbf{0} & \mathbf{0} \\ qI & qI & \mathbf{0} & \mathbf{0} \\ \mathbf{0} & \mathbf{0} & hC_f^T C_f & \mathbf{0} \\ \mathbf{0} & \mathbf{0} & \mathbf{0} & \mathbf{0} \end{bmatrix}, \ \Re = r\,I \tag{28}$$

The selected structure of $Q$ puts zero weight on the elements of the plant state, $x_p$, making the control system performance insensitive to the stator flux estimation errors. The weighting factors $q$, $h$, and $r$ are arbitrary positive constants. Conceptually, $q$ puts weight on the output errors and $h$ puts weight on the output pulsations while $r$ puts weight on the control input. An analytical determination of these parameters to meet specified performance requirements is difficult. Therefore, a computer aided design procedure is employed in this paper to determine proper values of these parameters, based on a compromise between different performance factors (speed of response, overshoot, sensitivity to measurement noise, etc. ) using trial and error method.

The real time optimal feedback control that minimizes (26) under the constraint (24) is given by

$$u(k) = g_1 \sum_{i=0}^{k} \varepsilon(i) + (g_2 - g_1)\varepsilon(k) + g_3 x_f(k) + g_4 x_p(k) + g_5 u(k-1) \quad (29)$$

The feedback gain,

$$G = [g_1 \quad g_2 \quad g_3 \quad g_4 \quad g_5] = -\Re^{-1} \Gamma^T H$$

is obtained by solving the Ricatti's equation

$$H\Phi + \Phi^T H - H\,\Gamma \Re^{-1} \Gamma^T H + Q = 0 \quad (30)$$

Provided that (*A, B*) is stabilizable and (*A, Q*) is detectable, the resulting closed loop system $x(k+1)=(A+BG)x(k)$ is asymptotically stable due to the property of LQ regulator design [24].

Equation (29) determines the rotor control voltage that minimizes the stator active and reactive power errors and attenuates their pulsations if existent.

Table 1 Modulating signals of different rejection control objectives

| Obj. no. | Pulsations to be rejected | $M_d$ | $M_q$ |
|---|---|---|---|
| (0) | Non | 0 | 0 |
| (1) | Active and reactive power | $P_s$ | $Q_s$ |
| (2) | Torque and reactive power | $\frac{\omega_e}{n} T_{em}$ | $Q_s$ |
| (3) | Stator current | $V_{s0} i_{sd}$ | $-V_{s0} i_{sq}$ |
| (4) | Rotor current | $-V_{s0} \frac{L_m}{L_s} i_{rd}$ | $\frac{V_{s0}}{L_s}(\frac{V_{s0}}{\omega_e} + L_m i_{rq})$ |

## 5. Disturbance Rejection Control Objectives

The filter input signals, considered so far, are the stator active and reactive power, see (21). More specifically, the filter input signals are two signals having average values equal to the stator average active and reactive power, respectively, and modulated with their pulsations required to be attenuated. This concept can be generalized by using any two signals $M_d$ and Mq having average values of the stator active and reactive power, respectively but modulated with the pulsations of any other variable (torque, stator current, or rotor current) that need to be attenuated. From the DFIG mathematical model, (1)-(6), a number of equations relating the stator average active and reactive power to other machine variables can be deduced. On that basis, different disturbance rejection control objectives can be realized using the modulating signals listed in table 1 where $T_{em}$ is the electromagnetic torque and *n* is the number of pole pairs.

To make the performance of the disturbance rejection control loop independent of the fault type, the filter transfer function, $H_f(p)$ & $p=d/dt$, is selected such that it has poles at $\pm j\omega_e$ and $\pm j(2\omega_e)$ as

$$H_f(p) = C_f(pI - A_f)^{-1} B_f = \begin{bmatrix} \frac{4\omega_e^4}{p^4 + 5\omega_e^2 p^2 + 4\omega_e^4} & 0 \\ 0 & \frac{4\omega_e^4}{p^4 + 5\omega_e^2 p^2 + 4\omega_e^4} \end{bmatrix} \quad (31)$$

## 6. System Evaluation

Simulation studies are carried out on 2 MW DFIG whose parameters are listed in the appendix. The control system is implemented on the basis of Fig. 6 using the Matlab™ programming environment. The stator active and reactive powers are determined from the measured stator currents and voltages using the instantaneous power theory [25]. A position encoder is used to measure the rotor position $\theta_r$ while a phase looked loop (PLL) circuit is employed to determine the stator voltage vector angle $\theta_e$. The stator flux vector is estimated in the stationary ($\alpha\beta$) frame by substituting $\omega_e=0$ in (1). On the basis of (29), the rotor control voltage is determined and transformed to the rotor ($\alpha'\beta'$) frame using slip angle $\theta_s = \theta_e - \theta_r$. The switching pulses of the rotor-side converter are generated utilizing the space vector pulse width modulation (SVPWM) technique with 2 kHz switching frequency. The DC-link voltage $V_{dc}$ is kept constant under the influence of control of the grid-connected converter where 40mF DC-link capacitance is assumed.

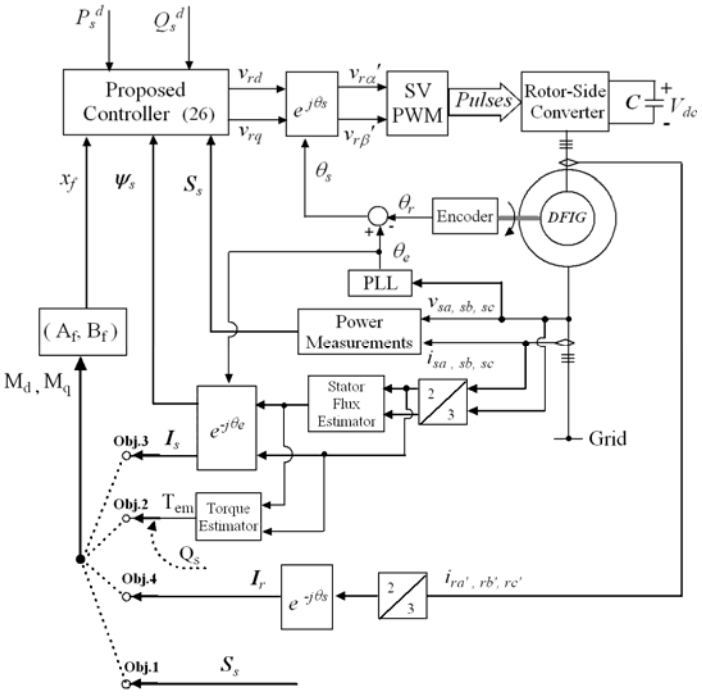


Fig. 6 Block diagram of the proposed control scheme

In the simulation, two sets of weighting factors are considered; set A comprises q=h=100, r=$10^{10}$ whilst, set B includes q=h=1, r=$10^{10}$. In the following, the different rejection control objectives will be indicated by their numbers as in Table1.

### 6.1 Normal Grid Condition

A study of the control system performance during normal grid voltage condition is carried out. Fig. 7 shows the simulated system responses to step changes in the power references at a fixed rotor speed of 1pu with the two sets of weighting factors and $M_d$ and $M_q$ as in Obj. no.4. In both cases, the steady state errors are negligible; however the effectiveness of the proposed control is clearly indicated in Fig. 7a. Where, by increasing the weight on the output errors, fast dynamic response of both the stator active and reactive power with good decoupling and small overshoot is obtained. On the contrary, small weight on the output errors yields sluggish dynamic performance and significant coupling between the active and reactive power control loops as depicted in Fig. 7b. The figure also demonstrates the rotor current responses where the same rules can be concluded.

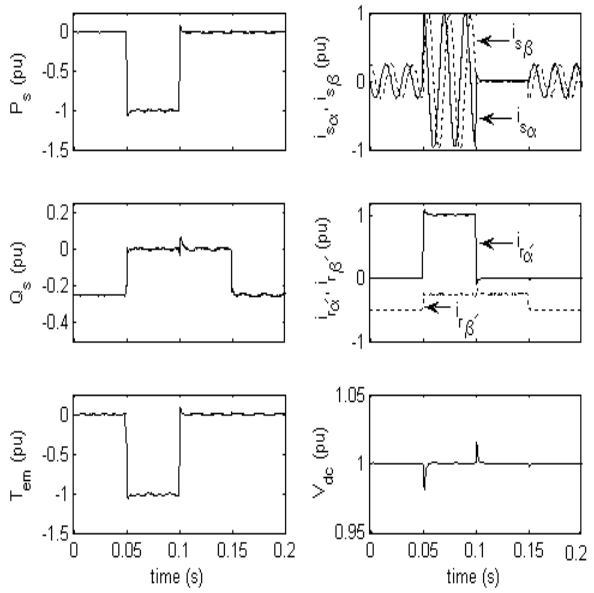


(a)

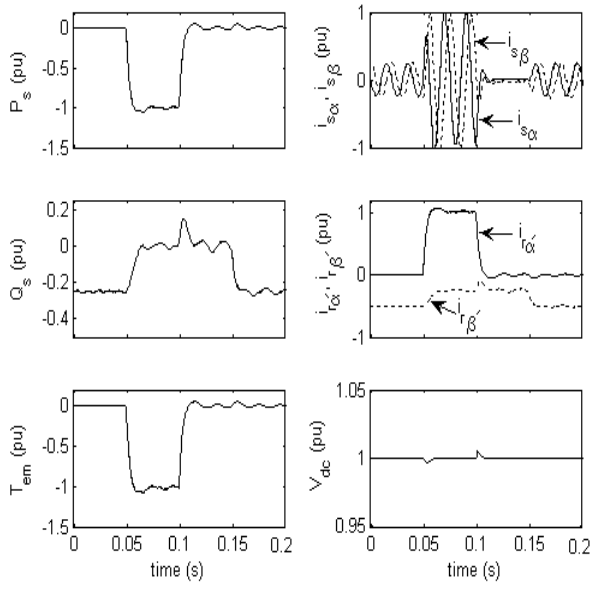


(b)

Fig. 7 Simulated results under step changes in the power references. (a) Set A {q=h=100, r=$10^{10}$}. (b) Set B {q=h=1, r=$10^{10}$}

Another test is carried out with the speed of the generator specified by external input simulating the torque from the turbine. Fig. 8 shows the simulated results when the input mechanical torque changed abruptly at t=0.25s

from 0.5 to 0.9pu with the weighting factors as in set A. The lumped inertia constant is set to small value in the study to reduce the simulation time. The rotor speeds up and the reference active power increases to achieve maximum power point tracking. Furthermore, the reactive power reference is changed from -0.25 to 0pu at t=1.5s. The figure reveals that the system operation is satisfactory during torque/speed variations.

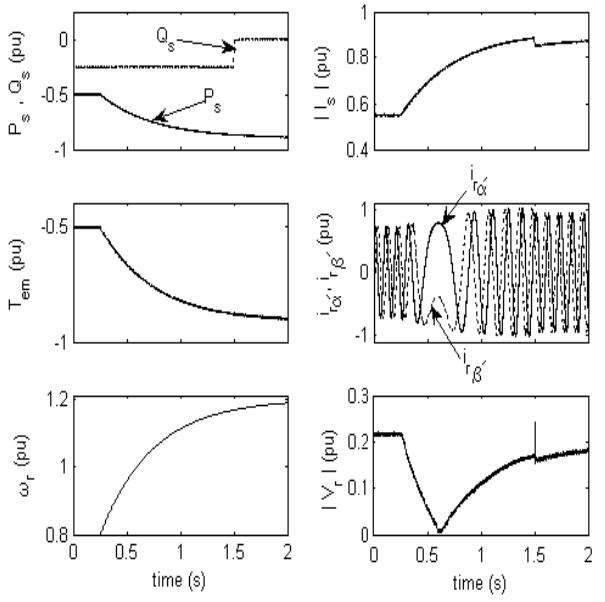


Fig. 8 Simulated results under torque/speed variations and with set A {q=h=100, r=$10^{10}$}

### 6.2 Grid Voltage Unbalance

The DFIG is most likely operating as part of a wind farm. To get better wind conditions and less planning restrictions, wind farms are usually located in remote rural areas where voltage unbalance commonly exists. Unbalanced grid voltage causes unbalanced currents to flow in the stator and rotor windings. As a result, double frequency power and torque pulsations will be produced. The unbalanced currents create unequal heating on the machine windings, the torque pulsations can be a source of excessive mechanical stress on the wind turbine while the power pulsations tend to magnify the grid voltage unbalance [10-11]. Accordingly, the capability of the proposed control to alleviate the problems associated with the DFIG operation under grid voltage unbalance is an important feature.

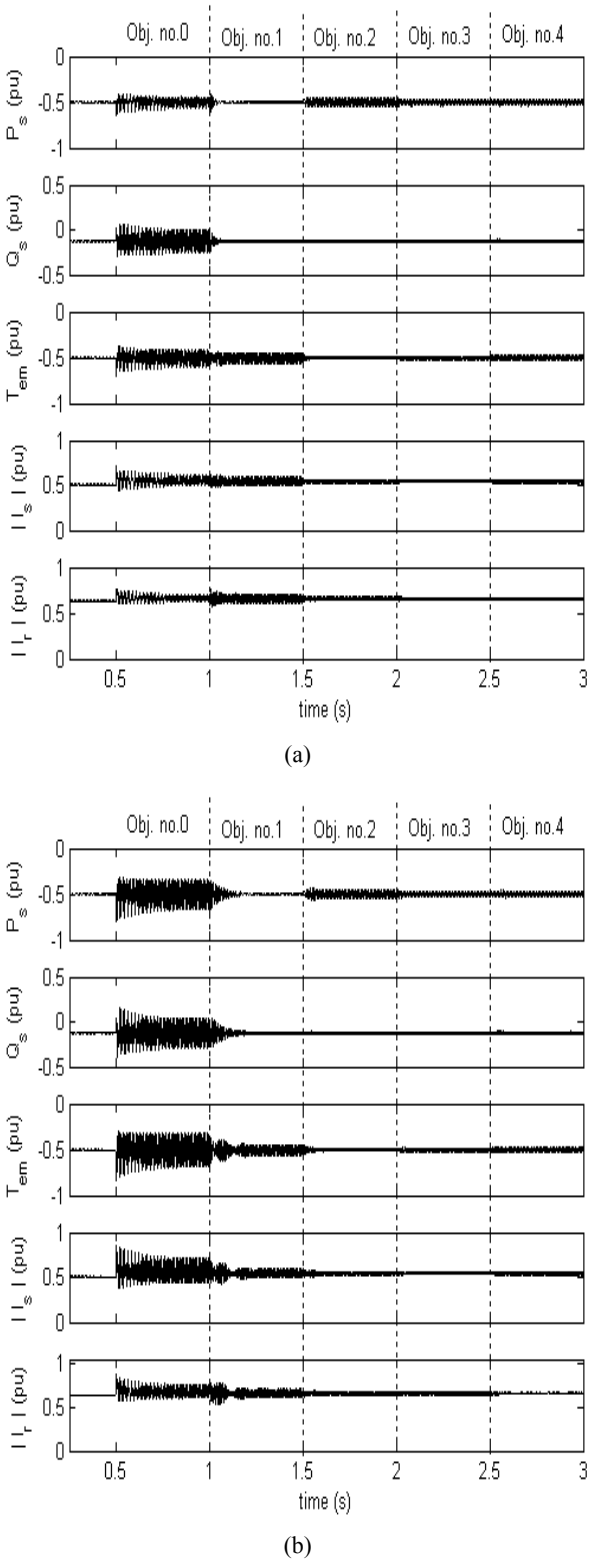


Fig. 9 Simulated results under grid voltage unbalance and different rejection control objectives. (a) Set A {q=h=100, r=$10^{10}$}. (b) Set B {q=h=1, r=$10^{10}$}

This capability is examined by assuming sudden reduction in the magnitude of a-phase voltage by 20% at t=0.5s while the generator delivers active and reactive power of -0.5 and -0.15pu, respectively, at constant rotor speed of 1pu. Fig. 9 shows the simulated responses with the two sets of the weighting factors and different rejection control objectives. No rejection for the generator variables pulsations (Obj. no.0) is applied from t=0-1s by setting $M_d$=0 and $M_q$=0. Rejection of the stator powers pulsations, torque and reactive power pulsations, stator current pulsations, and rotor current pulsations (obj. no.1, no.2, no.3, and no.4, respectively) are applied in sequence during the time intervals; 1-1.5s, 1.5-2s, 2-2.5s, and 2.5-3s, respectively. Examination of Fig. 9a and Fig. 9b reveals ` 1) Fast dynamic power control limits the transient currents under abrupt change in the grid voltage. 2) The speed of response of the power control reduces, but doesn't eliminate, the generator variables pulsations under grid voltage unbalance. 3) The disturbance rejection control is effective in achieving its objectives regardless of the performance of the power control loop. 4) Attenuating the rotor current pulsations (Obj. no.4) also reduces the stator powers, stator current, and electromagnetic torque pulsations compared with the case of no compensation (Obj. no.0). Furthermore, compensating the rotor current pulsations eliminates the unequal heating of the rotor winding as well as the unequal stress on the switching devices of the rotor-side converter.

### 6.3 Symmetrical Grid Fault

The severity of the grid fault depends on the fault type, prefault generator speed, and output power. The largest rotor current will flow in the case of sudden symmetrical 3-phase fault bringing the stator voltage down to a small value while the generator delivers full load power at super synchronous speed. Following the criteria in [15], the FRT is considered successful if the rotor current is confined within the safe operating area (SOA) of the rotor-side converter which is typically 100% higher than the continuous current rating. Therefore, the DFIG control objective is to constrain the instantaneous rotor current below 2pu just to keep the generator connected to the grid. Another objective for the grid-side converter control is to limit the DC overvoltage; however this is outside the scope of this paper.

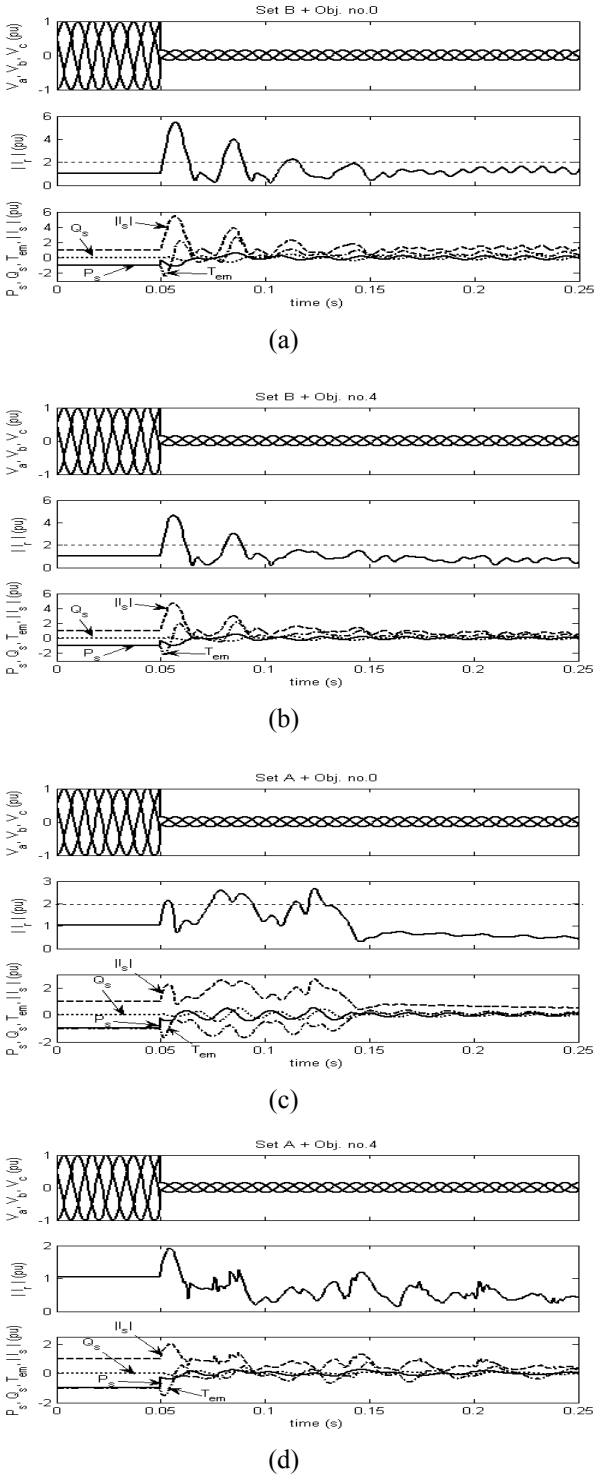


Fig. 10 Simulated results under symmetrical 3-phase fault. (a) Set B {q=h=1, r=$10^{10}$} and Obj. no.0. (b) Set B {q=h=1, r=$10^{10}$} and Obj. no.4. (c) Set A {q=h=100, r=$10^{10}$} and Obj. no.0. (d) Set A {q=h=100, r=$10^{10}$} and Obj. no.4

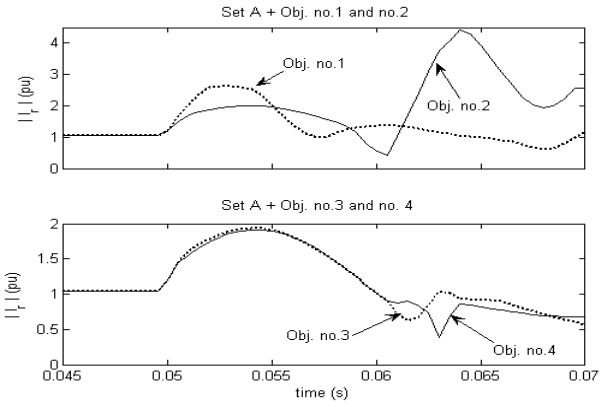


Fig. 11 Rotor current response under grid fault with Set A {q=h=100, r=$10^{10}$} and different rejection control objectives

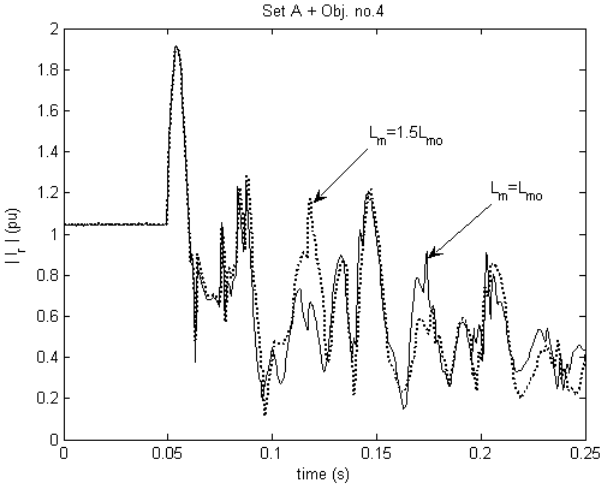


Fig. 12 Rotor current response under grid fault with nominal magnetizing inductance (solid) and a 50% step increase in the magnetizing inductance at t=0.05 (dotted)

Accordingly, the DC-link voltage is considered constant during this case study. The FRT capability of the proposed control is verified by assuming the generator initially delivering full load active power at 1.2pu super synchronous speed. A step reduction in the stator voltage from 1 to 0.15pu is considered at t=0.05s. Under the detection of the grid fault, the stator power references are set to zero, torque/speed control loop is deactivated, and no external action to limit the fault current is taken. Fig. 10 shows the simulated system responses for the two sets of the weighting factors with and without compensation of the rotor current pulsations. In case of slow dynamic control without compensation (Set B + Obj. no.0), the rotor fault current reaches to 5.7pu as shown in Fig. 10a. It is worthy to mention that higher fault current was reported in case of traditional rotor current vector control [15]. By applying the rejection control of the rotor current pulsations with the same weighting factors (Set B + Obj. no.4), the rotor fault current reduces to 4.7 pu as depicted in Fig. 10b. However, in both cases, the generator cannot stay connected to the grid and protection of the rotor-side converter is necessary.

By using fast power control without compensation of the rotor current pulsations (Set A + Obj. no.0), the first rotor current peak is reduced by considerable amount to be 2.2pu as demonstrated in Fig. 10c. A further increase in the rotor fault current after the first peak is noted as a result of pronounced swinging in the power outputs. On the other hand, full compatibility with the FRT requirements is obtained by employing fast power control and attenuation of the rotor current pulsations (Set A + Obj. no.4) as depicted in Fig. 10d. As shown in that figure, the rotor fault current is about 1.9pu and the tendency of further increase is eliminated. Fig. 11 shows the rotor current responses under the same fault conditions with fast power control (Set A) and different rejection control objectives. It is evident that attenuating the power or torque pulsations (Obj. no.1 & no.2) are not adequate strategies for this fault scenario. Thus attenuating the stator current pulsations or the rotor current pulsations (Obj. no.3 & no.4) gives satisfactory results with slight improvement in the latter.

The robustness of the proposed control to parameter variations is verified in Fig. 12. Under the same fault conditions, the rotor current response with constant magnetizing inductance at the nominal value is plotted in solid lines while the rotor current response with a 50% step increase in the magnetizing inductance at t=0.05s is demonstrated in dotted lines. It is clear that the FRT capability of the proposed control is insensitive to the magnetizing inductance variations.

## 7. Conclusion

This paper presents a novel stator power model for the DFIG. The model considers all the generator dynamics and provides a means of direct stator power control. Brief

analysis of the DFIG performance under grid faults is carried out. Attenuation of the rotor current pulsations is proposed to improve the FRT capability and overcome the difficulties of estimation of the stator flux transient component. On the basis of the derived model, a new robust optimal state controller with narrowband disturbance rejection is synthesized. Attenuation of a number of choices of the generator variables pulsations is realized. Simulation studies have been carried out on 2MW DFIG to validate the proposed control under normal and abnormal grid voltage conditions. The results showed that, with compensating the rotor current pulsations, the control system can satisfy the following requirements: 1) Fast direct power control while maintaining the system stability 2) Mitigation of the problems associated with the generator operation under unbalanced grid voltage. 3) Successful FRT considering severe prefault operating conditions.

These features are very important for the DFIG-based wind turbine which suffers from limited stability margin, frequent grid voltage unbalance, and new stricter FRT requirements. The effectiveness of the introduced control method together with its simple structure and formal design procedure make it a viable solution for this application.

## Appendix

The simulated 2MW, 690V, 50 Hz, 4-pole, Y-Y, DFIG has the following equivalent circuit parameters: $R_s$ / $R_r$ = 0.00488 / 0.00549 pu, $L_s$ / $L_r$ = 4.0913 / 4.102 pu, $L_m$ = 3.9257pu, Stator/rotor turns ratio = 0.45, and the inertia constant = 3.5 s. The base values are taken as:

Base apparent power = 2 MVA, base voltage = 563.4 V, base angular frequency= 314 r/s, and the base DC voltage = 600V.

## References


[1] L. Gertmar, L. Liljestrand, and H. Lendenmann," Wind energy powers-That-Be successor generation in globalization," IEEE Trans. On Energy Conversion, vol. 22, no. 1, pp. 13-28, March 2007.

[2] American Wind Energy Association, "AWEA electrical guide to utility scale wind turbines," March 2005.

[3] R. Datta and V. T. Ranganthan," Variable speed wind generation using doubly fed wound rotor induction machine: a comparison with alternative scheme," IEEE Trans. On Energy Conversion, vol. 17, no. 3, pp. 414-421, Sept. 2002.

[4] S. Muller, M. Deicke, and R. W. De Doncker, "Doubly fed induction generator systems for wind turbines," IEEE Ind. Appl. Mag., vol. 8, no. 3, pp. 26-33, May/Jun. 2002.

[5] A. Peterson, "Analysis, modeling and control of doubly fed induction generators for wind turbines," Ph. D. dissertation, Chalmers Univ. of Technology, Gothenburg, Sweden, 2005.

[6] C. Abbey, J. Chahwan, M. Gattrell, and G. Joos, "Transient modeling and simulation of wind turbine generator and storage systems," CIGRA Canada, Conf. On Power systems, no. 042, pp. 3-8, Oct. 2006.

[7] L. Xu and C. Wei, " Torque and reactive power control of a doubly fed induction machine by position sensorless scheme," IEEE Trans. On Ind. Appl., vol. 31, no. 3, pp. 636-642, May/Jun.1995.

[8] B. Hopfensperger, D. J. Atkinson, and R. A. Lakin, "Stator flux oriented control of a doubly fed induction machine with and without position encoder," Proc. Inst. Elect. Eng., vol. 147, pp. 241-250, Jul. 2000.

[9] A. Petersson, L. Harnefors, and T. Thiringer," Comparison between stator-flux and grid-flux-oriented rotor current control of doubly-fed induction generators," in proc. Of PESC'04, pp.482-486, Aachen, Germany, 2004.

[10] T. Brekken, and N. Mohan, "Control of a doubly fed induction wind generator under unbalanced grid voltage conditions," IEEE Trans. On Energy Conversion, vol. 22, no. 1, pp-129-135, March 2007.

[11] L. Xu and Y. Wang, "Dynamic modeling and control of DFIG based wind turbines under unbalanced network conditions," IEEE Trans. On Power Systems, vol. 22, no. 1, pp 314-323, March 2007.

[12] J. D. Rose and I. A. Hiskens, "challenges of integrating large amount of wind power," 1st Ann. IEEE systems Conf., pp. 259-265, April 2007.

[13] G. Joos, "Review of grid codes," Int. Conf. on Integration of RE and DER (IRED04), Brussels, Belgium, Dec. 2004.

[14] R. Zavadil, N. Miller, A. Ellis, and E. Muljadi, "Making connections," IEEE Power & Energy Mag., vol. 3, no. 6, pp. 26-37, Nov./Dec. 2005.

[15] D. Xiang, L. Ran, P. J. Tavner, and S. Yang," Control of a doubly fed induction generator in a wind turbine during grid fault ride-through," IEEE Trans. On Energy Conversion, vol. 21, no. 3, pp. 652-662, 2006.

[16] H. Bankar, C. Lou and B. T. Ooi, "steady state stability analysis of doubly fed induction generators under decoupled P-Q control," IEE Proc. Electric Power Appl.,

vol. 153, no.. 2, pp. 300-306, 2006.
[17] M. Heller and W. Schumacher, 'Stability analysis of doubly-fed induction machines in stator flux reference frame," in Proc. of EPE'97, vol. 2, pp. 707-710, Torndheim, Noway, Sept. 1997.
[18] L. Congwei, W. Haiqing, S. Xudong, and L. Fahai, "Research of stability of double fed induction motor vector control system," in Proc. of ICEMS'01, vol. 2, pp. 1203-1206, Shenyang, China, Aug. 2001.
[19] A. Petersson, L. Harnefors, and T. Thiringer, "Evaluation of current control methods for wind turbines using doubly fed induction machines," IEEE Trans. On Power Electronics, vol.20, no. 1, pp.227-235, 2005.
[20] J. Holtz," Sensorless control of induction machines —with or without signal injection? " IEEE Trans. On Industrial Electr., vol. 53, no. 1, pp. 7-30, Feb. 2006.
[21] N. K. Gupta, "Frequency shaped cost functionals: Extension of linear quadratic Gaussian design methods," J. Guidance Contr., vol. 3, no. 6, 1980.
[22] Osama S. Ebrahim, Mohamed M. Negm and Mohamed Z. Youssef "An Improved DTC scheme for The AC Drives Based on Optimal Preview Control Technique," ISIE2006, July 2006.
[23] Mohamed M. Negm, Mohamed F. Salem and Osama S. Ebrahim," Experimental investigation of high performance induction motor control based on optimal preview controller," IEEE ICIT '04, Vol. 1, pp. 334-340, 2004.
[24] R. F. Stengel," Optimal control and estimation," Dover publications, New York, 1994, book.
[25] H. Akagi, S. Ogasawara, H. Kim, " The theory of instantaneous power in three-phase four wire_systems: a comprehensive approach," in proc. IEEE-PESC Conf., pp.431-439, 1999

**Osama S. Ebrahim** was born in Cairo, Egypt, in 1970. He received his B.E., M.Sc., Ph. D degrees in electrical engineering from Ain-Shams University, Cairo, Egypt in 1994, 1999, and 2004 respectively. From 2005-2006 he was a Lecturer in the same university. Since 2006, he has been a post doctor fellow in the Energy and Power Electronics Applied Research Laboratory (*e*PEARL), Queen's University, Kingston, ON, Canada. His research interest includes analysis and design of electrical machines, modern control theories and their applications to the electrical machines, electric power systems, and power electronics based energy conversion systems.

**Praveen K. Jain** (S'86–M'88–SM'91–F'02) received his B.E. (with honors) degree from the University of Allahabad, India, in 1980, and the M.A.Sc. and Ph.D. degrees from the University of Toronto, Canada, in 1984 and 1987, respectively, all in electrical engineering. He is a Professor and Canada Research Chair in Power Electronics at Queen's University in Canada where he established a multi-million dollar state-of-the-art *Energy* and Power Electronics Applied Research Laboratory (*e*PEARL). Prior to this, he was a Professor at Concordia University, a Technical Advisor with Nortel Networks, a Senior Engineer with Canadian Astronautics, a Design Engineer with ABB and a Production Engineer at Crompton Greaves. He also has considerable consulting experience with the industry. He has published over 300 technical papers and has 35 patents in the area of power electronics. His current research interests are power electronics applications to space, telecommunications, computer systems, and renewable energy resources. Dr. Jain is a Fellow of the IEEE, the Engineering Institute of Canada and the Canadian Academy of Engineers. He is the recipient of the 2004 Engineering Medal (R&D) of the Professional Engineers of Ontario. Dr. Jain is an Associate Editor of the IEEE Transactions on Power Electronics. In 2006, Dr. Jain founded CHiL Semiconductor in Boston that received $15M US in venture funding to commercialize intelligent digital power semiconductor products and is a Chief Technology Officer and a Director of the Board.

**Goel Nishith** received his B.E. (with honors) in electronics and telecommunications engineering from the University of Jodhpur, India; his M.A. in electrical engineering and his Ph.D. degree in systems design engineering from the University of Waterloo, Canada. In 1984, he joined Bell-Northern Research (Nortel Net-works) as a member of the scientific staff. He worked at Nortel Networks for over 12 years. During that time, he worked in various groups in semiconductor design and manufacturing. In 1995, he founded Cistel Technology. Cistel is an Information Technology and Engineering Consulting Company and also engaged in research and product development. Since then, the company has expanded to over 130 employees and consultants with offices in Ottawa, Toronto, Atlanta (USA) and New Delhi (India).